

# ***Recordings of Long-Period Fluctuations Associated with the Passage of Three Distinct Tsunamis at Broadband Seismometers Made at the International Monitoring System (IMS) Hydroacoustic T-station H06 (Socorro Island, Mexico)***

**by Alexander S. Poplavskiy and Ronan J. Le Bras**

## **INTRODUCTION**

In the wake of the very large Indian Ocean tsunami on 26 December 2004, and several subsequent events in the Pacific Ocean, scientific and disaster mitigation studies have been initiated to better understand and observe tsunami propagation. This paper describes observations made on nearshore long-period seismometers of a little known and, to our knowledge, recently discovered phenomenon associated with the passage of tsunamis near a coast. It provides further insight into this phenomenon. Observations of long-period effects of the passage of tsunamis on the horizontal components of nearshore seismometers were initially made by [Yuan \*et al.\* \(2005\)](#). A quantitative assessment was first made by [Okal \(2007\)](#). These observations were made on the Indian Ocean tsunami of December 2004. We observe similar long-period oscillations for the tsunamigenic Maule, Chile, earthquake of 27 February 2010 at two broadband seismometers used as hydroacoustic T-station of the International Monitoring System (IMS) network and located on Socorro Island, Mexico. Polarization and amplitude analysis of the long-period arrivals on the two closely spaced seismometers allows us to propose an explanation for the polarization of observations that were not explained in [Okal \(2007\)](#). Our preferred interpretation of the phenomenon is that the surface of the island close to the shore is tilted by the loading from the local sea elevation change due to the passage of the long-wavelength tsunami wave. Whereas Okal ignores the presence of the island in his physical analysis, this tilting of horizontal seismic sensors induced by this slow dynamic process explains observations from several tsunamis and we would expect similar observations on near-coastal continental stations. This hypothesis is confirmed by the quantitative assessment and the analysis of the data at the two broadband seismometers during the passage at Socorro of other

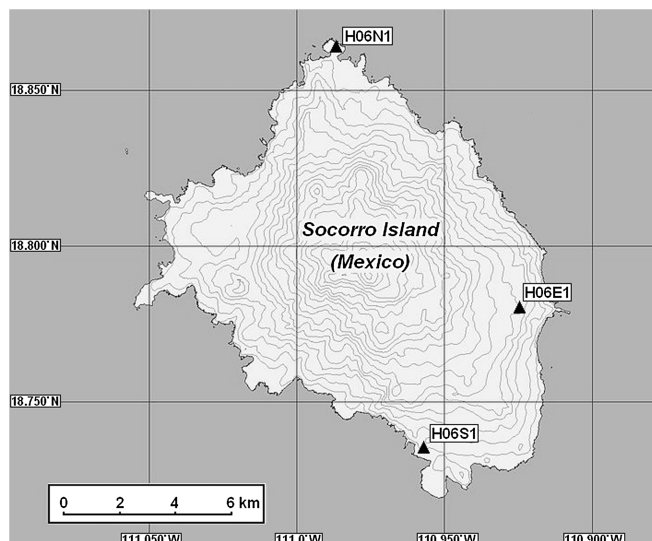
tsunamis from the 29 September 2009 Samoa earthquake, and from the catastrophic Japanese earthquake on 11 March 2011.

While examining seismic and hydroacoustic waves generated by the 27 February 2010 Maule, Chile, earthquake at IMS T-station H06, we observed long-period waves accompanying the passage of the tsunami generated by the earthquake. These long-period waves were observed principally on horizontal components. Similar observations at near-coastal seismometers had been made by [Yuan \*et al.\* \(2005\)](#), [Hanson and Bowman \(2005\)](#), and [Okal \(2007\)](#), for the 24 December 2004, Sumatra event, including the observation that the polarization of these waves is perpendicular to the coastline closest to the seismometers. To our knowledge, the most complete interpretation of these fluctuations is presented in [Okal \(2007\)](#). The author interprets the amplitude and period of the fluctuations, depending on the distance to the tsunamigenic source and the proximity of stations to the shoreline. Okal presents a statistical analysis of seismic recordings of low-frequency fluctuations of several tsunamis on coastal three component (3C) stations. Using these various observations, the author proposes that the instruments are responding to the combination of horizontal displacement, tilt, and perturbation in gravity described by [Gilbert \(1980\)](#). They are induced by the passage of the tsunami wave over the ocean basin. In this approximation, Okal simply ignored the island or continent structure, and assumed that the seismometer functions as an ocean-bottom instrument. According to this model, the direction of ground particle motions should coincide with the main direction of propagation of the tsunami waves. [Yuan \*et al.\* \(2005\)](#) also observe that the direction of polarization is toward the closest shore and explain the horizontal fluctuations via two possible mechanisms: passage of the gravitational tsunami wave recorded at the seismometers, and/or tilt of the coastal area of the island or continent due to a local loading by the passage of the gravity wave. The authors did not make a quantitative assessment of recorded low-frequency

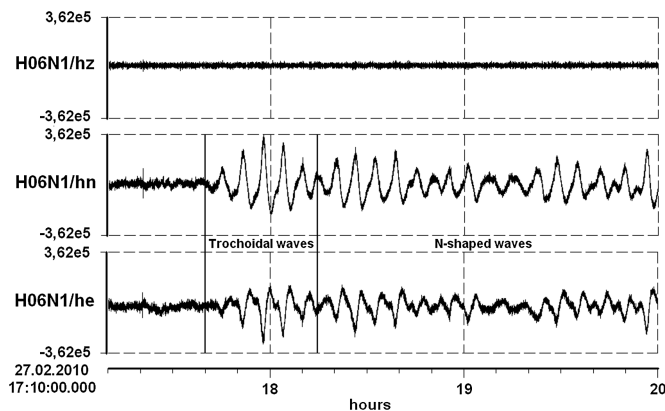
fluctuations, perhaps because they had been recorded by solitary 3C seismic stations and the local data density was not sufficient to distinguish the two effects, but made the observation that the latter phenomenon is the most likely because of the observed polarization. We believe that our observations further confirm that indeed the latter phenomenon, that is, a local coastal loading phenomenon is indeed dominant. The confirmation is made possible because the two broadband seismometers are located within a few kilometers (about 11 km) of each other on the same island. The research described in this work is a further confirmation that the sphere of application of coastal T-stations can be extended to the observation of the passage of tsunami waves.

## OBSERVATIONS

T-stations in the IMS are intended to detect hydroacoustic phases propagating in the oceans. The system distinguishes between two types of hydroacoustic phases. *T* phases originate from underground and couple into the water. *H* phases are generated by in-water explosions. Observation of one or the other of these phases helps in identifying the source. T-stations are not as sensitive as in-water hydrophones. They do observe *T* phases and *H* phases, but from higher-energy sources than hydrophones do, and it is difficult to assign an azimuth for the direction of propagation, which impedes the identification of source locations (Prior *et al.*, 2010). Their usage as standard seismic stations is also hampered by the high broadband noise from surf because they are located close to shore. IMS T-stations are placed on the coasts of islands and archipelagoes of the Pacific, Indian, and Atlantic oceans. T-station H06 consists of two broadband three-component Streckeisen STS-2 (H06N1 at 18.8616° N, 110.9861° W, H06E1 at 18.7805° N, 110.9253° W) seismic sensors, and one extremely short-period three-component sensor GS13 (H06S1 at 18.7347° N, 110.9575° W), located on opposite sides of Socorro Island, Mexico (see Fig. 1) that belongs to the Revillagigedo Archipelago. The island has an elongated northwest–southeast shape with maximum dimensions of about 15 × 15 km in the north–south and east–west directions. Socorro is the emergent peak of a large basaltic shield volcano that rises from the sea floor at a depth of ~3000 m. Its highest elevation is Mount Evermann at 1050 m above mean sea level. The island’s average submarine slope is a little less than 10° (Valenzuela *et al.*, 2007). The Rayleigh waves generated by the event were very well recorded at the two broadband seismometers, H06E1 (east) and H06N1 (north). The large displacement thrust faulting at the source of the event is an efficient generator of Rayleigh waves and these were very clearly observed at station H06. Outside of the very minor time shift expected between the two seismometers, the Rayleigh waves recorded at the neighboring stations H06E1 and H06N1 are nearly identical to each other in phase and amplitude. This observation confirms the correct calibration and good state of functioning of all components of the two broadband seismometers. When looking at the raw seismograms at station H06N1 (see Fig. 2), long-period quasi-harmonic waves were strikingly observed on the horizontal channels starting at



▲ **Figure 1.** Location of the broadband seismometer components of IMS T-station H06 on Socorro Island, Mexico. MARPLOT® map adapted from: [http://en.wikipedia.org/wiki/File:Socorro\\_Island\\_-\\_Marplot\\_Map\\_\(1-100,000\).jpg](http://en.wikipedia.org/wiki/File:Socorro_Island_-_Marplot_Map_(1-100,000).jpg) (last accessed March 2013). MARPLOT is developed jointly by the National Oceanographic and Atmospheric Administration (NOAA) and the Environmental Protection Agency (EPA).



▲ **Figure 2.** Long-period fluctuations at station H06N1 beginning at the expected arrival time of the initial tsunami wave from the Maule event, observed on the raw broadband seismograms. Note that the wave pattern is seen on the horizontal components (channels *he* and *hn*), with no indication of their presence on the vertical component (channel *hz*).

17:40 UTC, which corresponds to the expected time of arrival of the first waves from the tsunami. Their amplitude would be in the 1–10 millimeter range if we were to interpret them as horizontal displacement (frequency band 0.001–0.004 Hz); however, our preferred interpretation is that they are a manifestation of ground tilt.

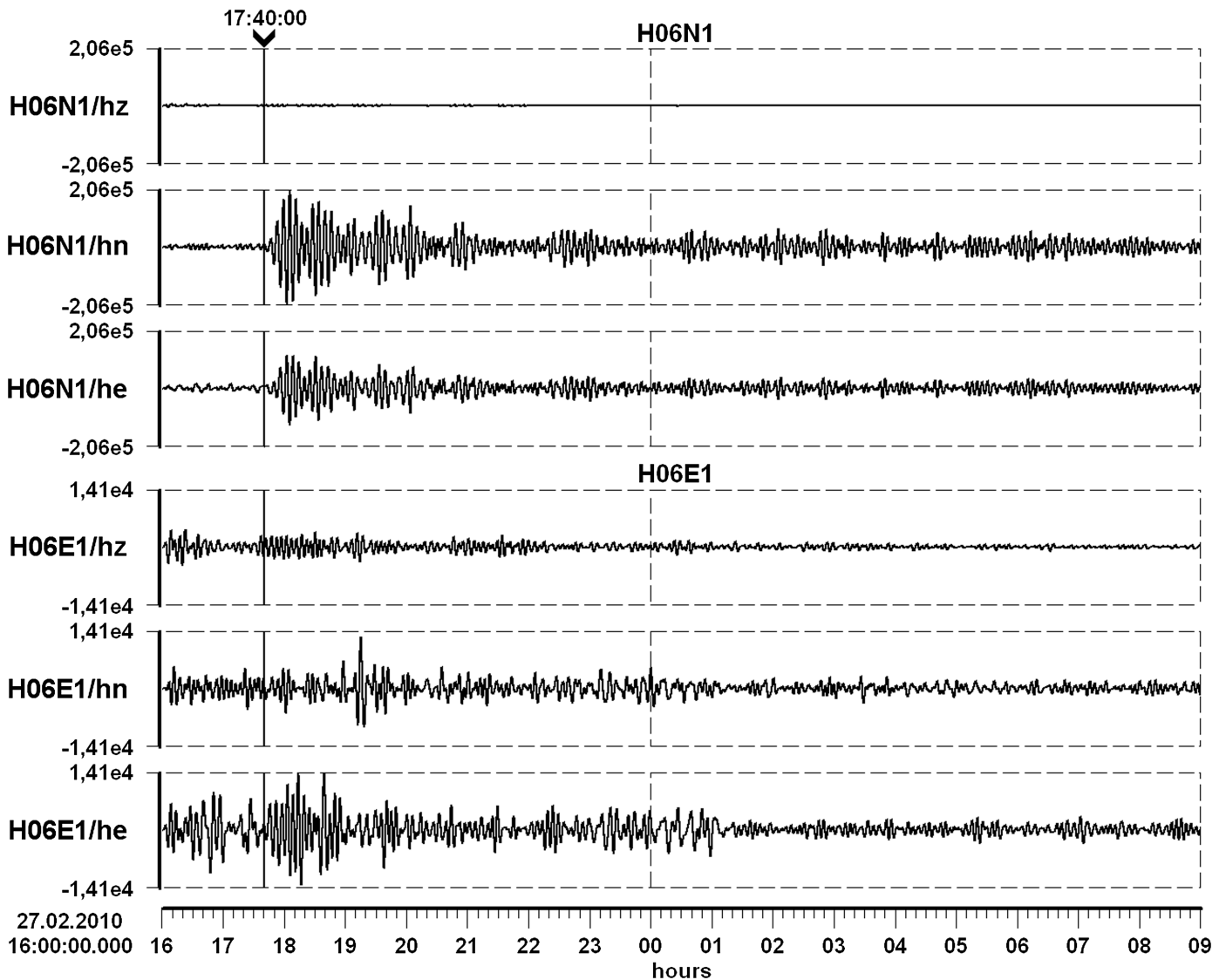
The dominant period of the quasi-harmonic fluctuations is approximately 350–420 s, very uncharacteristic of seismic

waves. Fluctuations with the similar period of 380 s were also observed at the H06E1 seismometer, located 11 km to the southeast of H06N1. The amplitude of the long-period waves at H06E1 is much lower, however. A third location at Socorro Island, H06S1 (south), is equipped with a short-period seismometer and did not observe these long-period arrivals.

Figure 3 shows the band-pass-filtered records respectively at stations H06N1 and H06E1. The filter band is 0.001–0.004 Hz (250–1000 s) and is optimized for the dominant frequencies of the signal. The time window is increased to 17 h to illustrate the long duration of the oscillations on the horizontal channels of station H06N1. The fluctuations continued with decreasing intensity throughout the next day, 28 February. The onset of the long-period arrivals occur at about the same time on station H06E1 as on station H06N1. It is prominent only on one of the horizontal channels (he) and the amplitude is lower than at the northern station. The interfer-

ence of the Rayleigh waves traced on the vertical channel from one of numerous aftershocks of the Chilean earthquake complicates the interpretation. The duration of the wave train observable at that station is only about one hour, the later arrivals being likely of too low amplitude to be observed in the noise background.

One question stemming from these observations at the two broadband stations is, how do we explain the physical process that causes such different behaviors of long-period waves at close-range stations? The first conclusion is that, without doubt, we are not observing long-period teleseismic waves which should be recorded identically by both stations. Because we are observing a phenomenon which is concomitant with the arrival of the tsunami wave in the ocean, we analyze the essential differences between these stations. One difference is the distance from the shoreline. For station H06E1, the distance is 1 km, for station H06N1, it is much closer, only 50 m.



▲ **Figure 3.** Long-period observations record at stations H06N1 and H06E1 in the 0.001–0.004 Hz frequency band from the Maule event. The time of the beginning of fluctuations is marked by the cursor.

The most probable source of the long-period fluctuations detected at station H06N1 is a phenomenon related to the passage of the strong tsunami by the island. The mainshock of the Chilean earthquake generated a strong tsunami that began to propagate across the entire Pacific Ocean. IMS hydroacoustic station H03 located on Juan Fernandez Island approximately 700 km offshore Chile was destroyed by the tsunami. The tsunami propagation in the Pacific basin was recorded at tide gauges monitored at the Tsunami Warning Centers. Many observatories provide data to the centers; such as the NOAA National Ocean Service, the University of Hawaii Sea Level Center, the Chilean Navy, and the National Tidal Center in Australia among others. The Preparatory Commission for the Comprehensive Nuclear-Test-Ban Treaty Organization (CTBTO) also provides auxiliary seismic data and hydroacoustic data to the Tsunami Warning Centers.

The estimated time of the arrival of the tsunami wave train to the Socorro Island coast, 16:54, is earlier than the onset time of the long-period fluctuations at stations H06, 17:40. This 30 min delay for the Chilean tsunami is also observed on offshore Japan GPS buoys and in the paper by Kato *et al.* (2011). They mention that several factors could cause the difference in arrival times including the sea-bottom topography on the path of tsunami propagation, the spatial resolution of gridding of their numerical calculations for the shorter wavelengths in the models, modeling errors, and so forth. The analysis of the bathymetry near Socorro defined that the island lies in the vicinity of the underwater mountain ridge stretching north–south for several hundred kilometers. The presence of the ridge may cause a slowdown of the propagation speed along the path from the Chilean coast, although the direct path is not directly over the ridge. On the basis of the average speed, the wavelength of the tsunami at station H06N1 is 70 km, but it is only a local estimate.

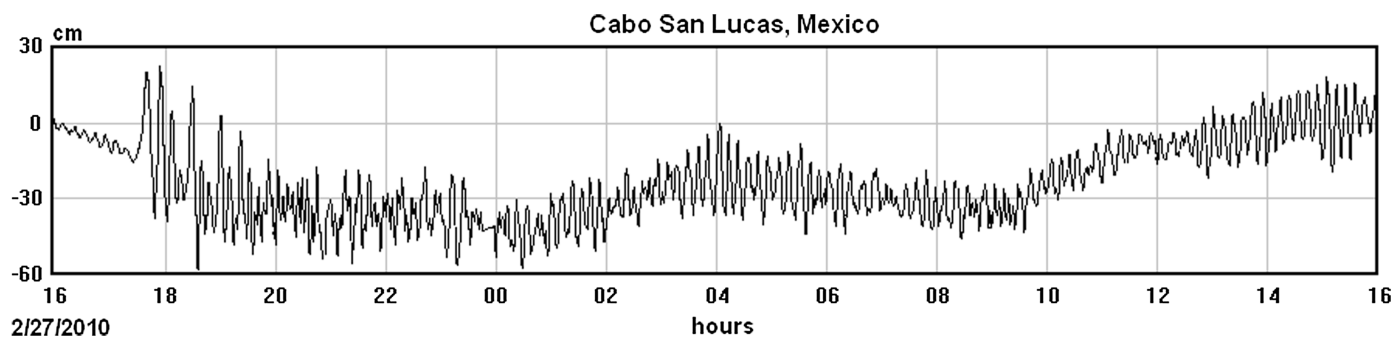
Figure 4 shows the tsunami record at the tide gauge at Cabo San Lucas, Mexico, which is located close to Socorro Island and belongs to the Deep Ocean Assessment and Reporting of Tsunamis (DART) Project from NOAA. The very long period fluctuations resembling instrumental drift are the oceanic tidal

fluctuations of sea level (Pan, 1971). The similarity in the overall duration and signal-to-noise ratio of the fluctuations at the tide gauge at Cabo San Lucas with the records of the horizontal channels of the station H06N1 (Fig. 3) is striking. The dominant frequency, however, is lower, in the range of 10–18 min, and the peak-to-trough amplitude is 50–60 cm. These differences are quite explainable. Close to shore, the speed of propagation and the wavelength decrease and the height increases. Using an approximate value of 18 min for the period of the tsunami offshore Socorro Island, the wavelength of a tsunami wave is approximately 200 km. Thus, the unique location and equipment of station H06N1 allows effective detection of not only *T*-phases and seismic waves in the short-period pass-band, but also observation of a long-period phenomenon associated with the passage of the tsunami near the island.

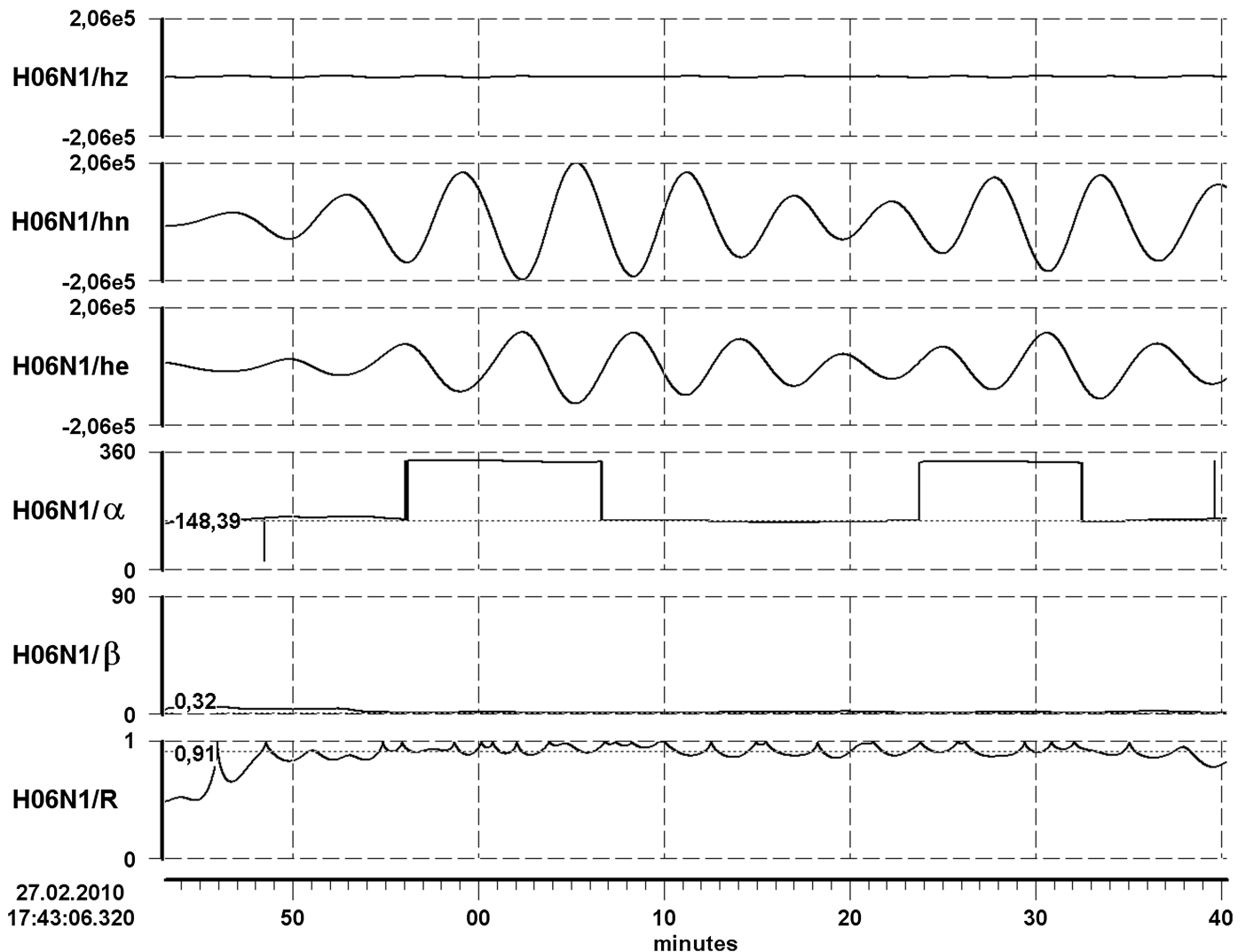
## POLARIZATION ANALYSIS

Polarization analysis of the three-component records of the long-period fluctuations at T-stations affords additional information about the orientation and linearity of the process and helps identify the physical process explaining the observations. For this purpose we applied the differential polarization analysis method developed by Shevchenko (2002). This analysis is adapted for the processing of the long-period seismic records with high time resolution and accuracy. The result of the polarization analysis of an initial record of fluctuations at the northern station using an algorithm initially developed to estimate the polarization of *P* waves is presented in Figure 5. The top three graphs show the three components at the same amplitude scale. The result of the calculation of the azimuthal function  $\alpha(t)$ , an inclination angle  $\beta(t)$  and rectilinearity  $R(t)$  are shown below the filtered data.

The calculated back azimuth of 148° corresponds with high accuracy to the direction to the source of the tsunami: the earthquake in Chile; the true value, using the National Earthquake Information Center (NEIC)-published epicenter, is 147°. We will see later, however, that this observation is pure coincidence. On the azimuthal estimation, occasional jumps of



▲ **Figure 4.** The tsunami record for the Maule event observed at the tide gauge in Cabo San Lucas, Mexico. The data, from the station operated and maintained by Centro de Investigación Científica y de Educación Superior de Ensenada (CICESE), Mexico, was adapted from the public web page of the Intergovernmental Oceanographic Commission (IOC) of the United Nations Educational, Scientific, and Cultural Organization (UNESCO): <http://www.ioc-sealevelmonitoring.org/station.php?code=cabo> (last accessed March 2013).



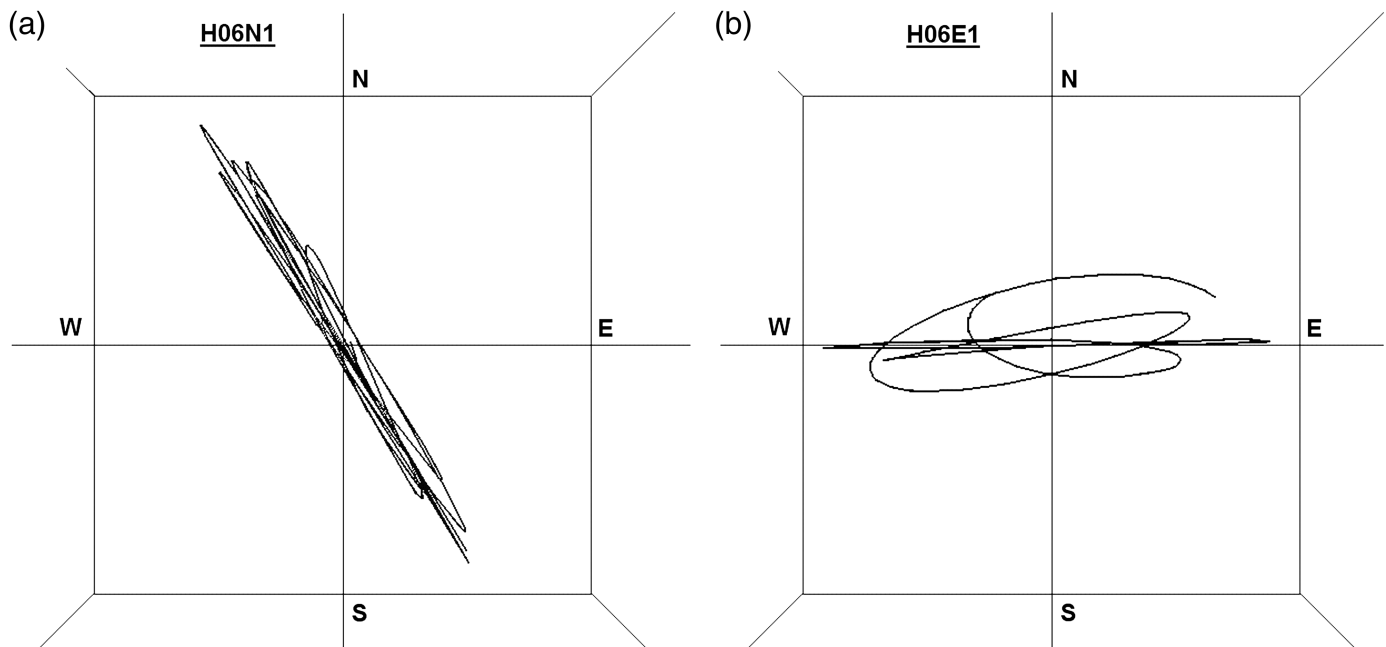
▲ **Figure 5.** Polarization analysis of long-period fluctuations at station H06N1 in the 0.001–0.004 Hz frequency band.

18° are observed. They are due to the 180° ambiguity because the inclination angle is near zero as the fluctuations occur only in a horizontal plane. The rectilinearity of the wave train is very high  $R \sim 0.9$ , which is often observed on records of longitudinal  $P$  waves. Throughout the duration of the tsunami-related wave train, the polarization direction remains very stable. This is an argument in favor of unequivocally attributing their origin to a single stable process. The hodograph of movements of the end of a vector of displacement for the displayed time window is shown in Figure 6a.

The polarization analysis on the northern station tends to allow drawing the conclusion that the direction of polarization corresponds to the direction of propagation of the tsunami. This is, however, not confirmed by examining the polarization of the data on the eastern station H06E (see Fig. 7). The estimation of the azimuth of polarization at the eastern station H06E1 is 89°. This direction is illustrated and confirmed by the hodograph of movements of the end of the displacement vector in Figure 6b, but in contrast to the hodograph

in Figure 6a, the particle motion of the eastern station has an elliptical shape rather than linear in direction of maximum amplitude. It confirms the rectilinearity function  $R$ , which is changing in a wide range and has maximal value over the interval of stability of functions  $\alpha(t)$  and  $\beta(t)$ . The inclination angle of the fluctuations is also close to zero, as for the northern station. Thus, results of the polarization analysis confirm the presence of an oscillatory process in the horizontal plane. However, owing to a low signal-to-noise ratio the fluctuations are not as striking as for station H06N1. We believe that the basic reason for the differences in the orientation of the fluctuations is the location of the stations. The direction of movement of particles appears to be perpendicular to the nearest coastline for both stations (see Fig. 8), in agreement with the observations of Yuan *et al.* (2005) mentioned above.

Polarization analysis shows that the vector of displacement is perpendicular to the nearest shoreline. When the sea level rises, the direction of displacement due to elastic deformations will point toward the inside of the island, along the direction of



▲ **Figure 6.** Particle-motion hodograph in the horizontal plane for the long-period fluctuations (0.001–0.004 Hz) at (a) station H06N1 and at (b) station H06E1 from the Maule event.

the applied pressure of water. The actual tilting will be toward the shore, however, the apparent displacement due to this tilt will appear to be directed toward the inside of the island. The comparison of raw seismic records shown on Figure 2 with the tsunami waves recorded by the DART tide gauges allows us to verify these conclusions. We next attempt a physical explanation.

## DISCUSSION

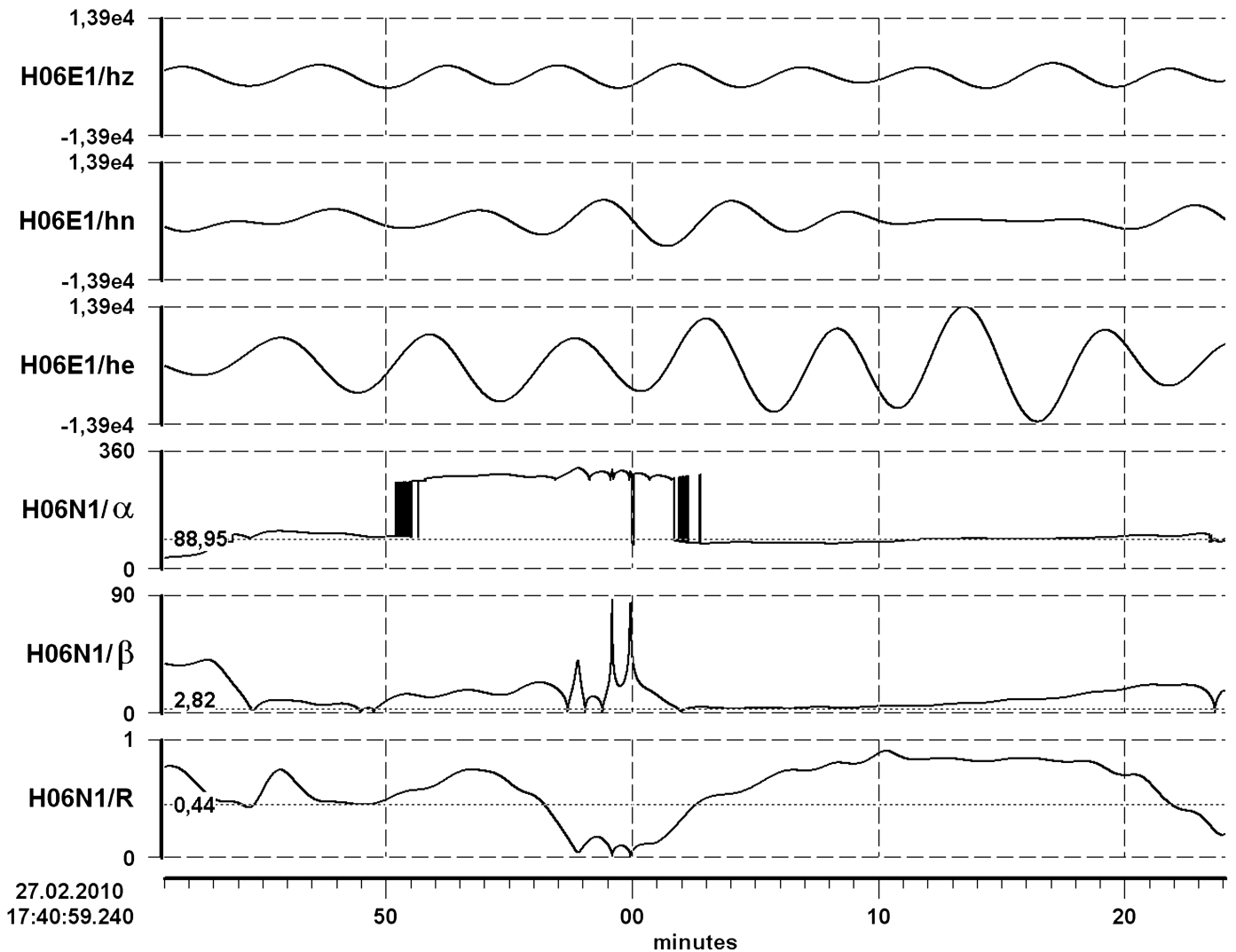
According to [Rodgers \(1968\)](#), the response of horizontal sensors  $\theta$  includes the following terms:

$$\theta = \theta_i + \theta_t + \theta_p, \quad (1)$$

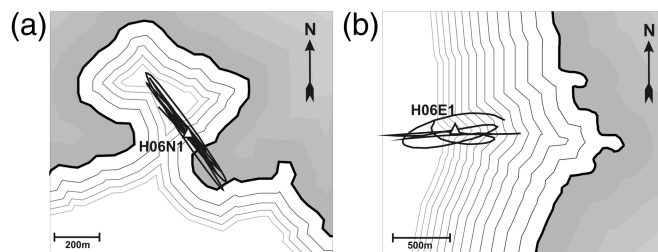
where  $\theta_i$  is an Ideal response, which would be expected from the seismometer if it were sensitive to the component of acceleration (velocity) along the horizontal axis;  $\theta_t$ , Tilt response, that is, affected by the inclination of vertical axis  $Z$  of the seismometer to the tilt angle  $\psi$ ,  $\theta_p$ , Parametric response, influenced by the free-period  $T_0$  of the seismometer. It tends to increase when the period of the input oscillation  $T$  is close to  $T_0$ . The seismic sensor STS-2 is designed to respond as a simple single-degree-of-freedom oscillator with free period  $T_0 = 120$  s, with differential feedback. However, the free oscillations at the resonance frequency of the sensor are effectively suppressed by a damping system. Therefore, for the observed fluctuations, the parametric response is negligible and we will ignore it. Thus, equation (1) simplifies to the sum of two terms: Ideal and Tilt response. We will examine the order of magnitude of each of these two responses to a local coastal loading. After comprehensive analysis of records of the DART system, [Bridg and](#)

[Demicco \(2008\)](#) note that waves become increasingly peaked (trochoidal), asymmetrical in profile, higher, and shorter, as they move into shallower water; they change from Airy waves to Stokes waves; some waves become solitary or N-shaped waves. Although we are looking at tilt rather than pressure, this description matches the observation on the raw records of horizontal channels of station H06N1 (Fig. 2), especially channel H06N1/he, where an initial wave train has an apparent trochoidal form with narrow sharp peaks and later wave trains resembling N-shaped waves. These trochoidal peaks correspond in time to the maxima of sea level. Their polarity on the horizontal channels is directed to the north and the west, that is, inside the island (see Fig. 8). This observation is compatible with both types of deformations, bulk compression or tilt.

For the purpose of illustrative and order of magnitude calculations, we choose typical values for Young's modulus for basalt ( $E = 75$  GPa) and height of the tsunami wave of  $H = 1$  m (the peak-to-peak amplitude value is 2 m). The estimated value for the displacement is then 16 microns. This is almost three orders of magnitude less than the observed value of 1–10 mm range at frequencies of 0.001–0.004 Hz, assuming that the sensor records displacement. Thus, the influence of elastic deformation is negligibly small and below the noise level. In addition, for this mechanism, we would also expect observations on the vertical components. It is therefore likely that the main generating mechanism for the observed fluctuations is a deformation leading to surface tilt, in agreement with the conclusions of previous authors on the topic. This also explains the absence of observations on the vertical channel. According to [Kalkan and Graizer \(2007\)](#) for small tilts, the amplitude of vertical oscillations is proportional to  $(1 - \cos \psi)$  and  $\cos \psi \approx 1 - \psi^2/2$ , and are therefore second order.



▲ **Figure 7.** Polarization analysis of long-period fluctuations at station H06E1 in the 0.001–0.004 Hz frequency band.



▲ **Figure 8.** Schematic model of possible tilt deformations in the coastal zone of (a) station location H06N1 and (b) H06E1. The space between isolines (on land) illustrates schematically the extent of inclination; a larger space between isolines corresponds to higher tilt angle at this site. The particle-motion hodograph overlaid on the site shows that the polarization direction is perpendicular to the isolines.

To relate the height of the tsunami to the observed tilt angle at the station, it may be best to assume a linear model  $H = f(\psi)$  and simply estimate empirically a factor  $k$  such that the water height  $H$  is given by the relationship:

$$H = k \cdot \psi, \quad (2)$$

where  $k$  is a conversion factor estimated in m/rad. It would be necessary to calibrate this  $k$  constant by having a tsunameter in the vicinity of the island, which was unfortunately not the case on 27 February 2010.

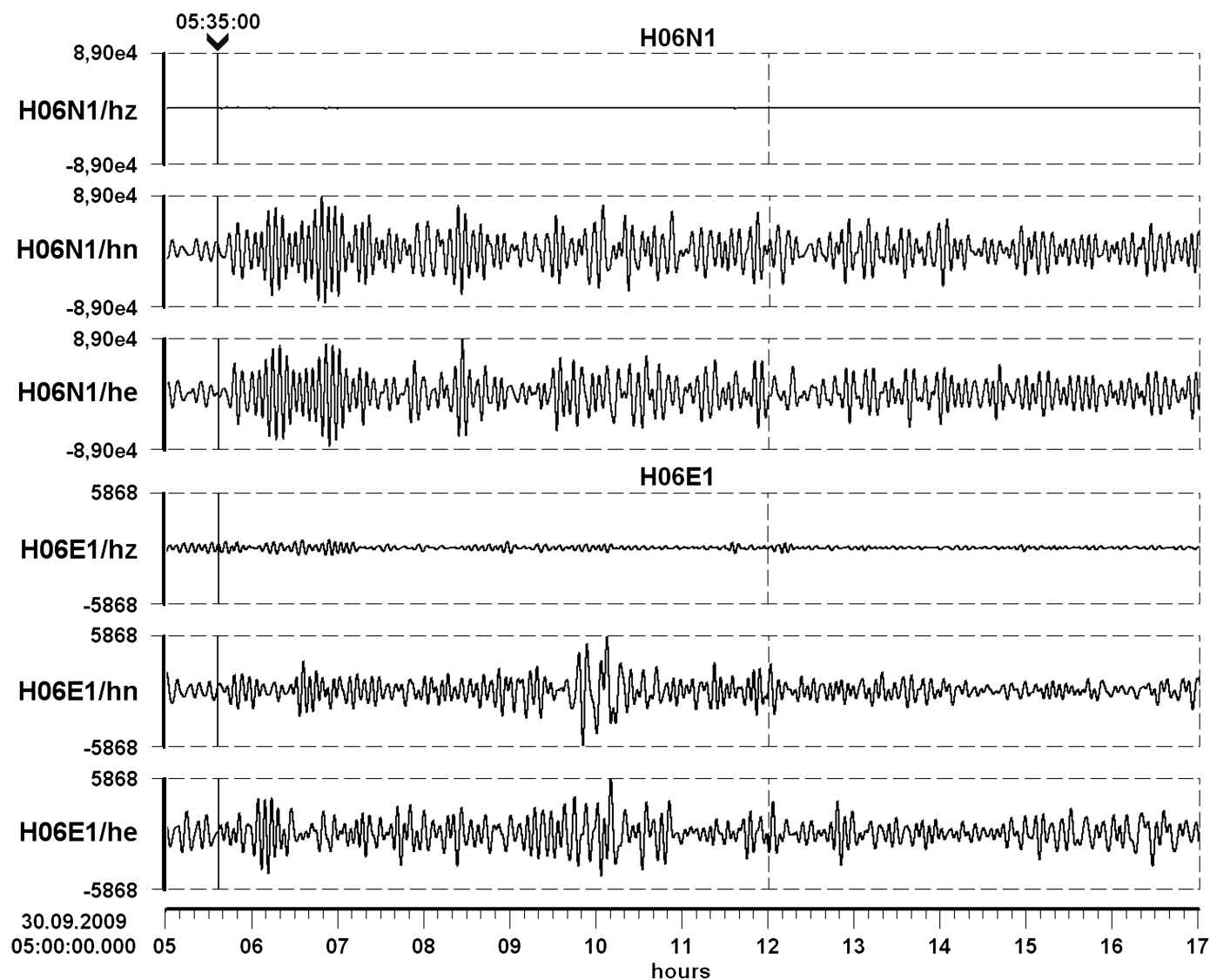
## OBSERVATIONS OF ADDITIONAL TSUNAMIS

The above interpretation of the very long-period fluctuations observed at the IMS H06 station lends itself to confirmation by the observation that similar phenomena as that observed during the passage of the tsunami generated by the Chilean Maule event should be observed during the passage of tsunamis

generated at other locations on the Pacific rim, because the mechanism we suggest for the generation of the fluctuation is independent of the direction of arrival of the tsunami wave train and essentially due to the vertical fluctuation of the ocean surface at the passage of the tsunami and the local coastal shape. Strengthened confidence in our interpretation was obtained by the observations of the H06 stations during the passage of the tsunami generated by the 29 September 2009, Samoa islands region earthquake (origin time 5:48:08 UTC). This earthquake is a very complex double event starting with a normal fault tear triggering an interplate slip by description of [Beavan \*et al.\* \(2010\)](#) with an  $M_w$  magnitude of 8.1 (according to USGS, <http://earthquake.usgs.gov/earthquakes/recenteqsww/Quakes/us2009mdbi.php>, last accessed March 2013). The distance from the source to station H06 is very similar to the Chilean source, 65.5° and 69°. The wave patterns of short-period seismic records are also similar: a powerful transversal  $S$  wave

and a surface Rayleigh wave are characteristic for a tsunamigenic event. As in the Maule event case, the earthquake generated a tsunami that propagated across a large portion of the Pacific Ocean. The initial wave height value at the source is about 3–4 m on the open ocean ([Fritz \*et al.\*, 2011](#)). Long-period fluctuations from the tsunami waves have successfully been detected on the horizontal channels of station H06N1. Long-period records at stations H06N1 and H06E1 in the 0.001–0.004 Hz frequency band are presented in Figure 9. As in the Maule event case, the fluctuations continued with decreasing intensity over the entire day. Similar fluctuations with considerably smaller amplitudes are recorded at station H06E1.

The onset time of the long-period fluctuations at the stations is 05:35 UTC the day after the event. The time of propagation of the tsunami from the source to the island is 11 h and 47 min and corresponds well with the expected time. Proceeding from this value, the average speed of propagation of



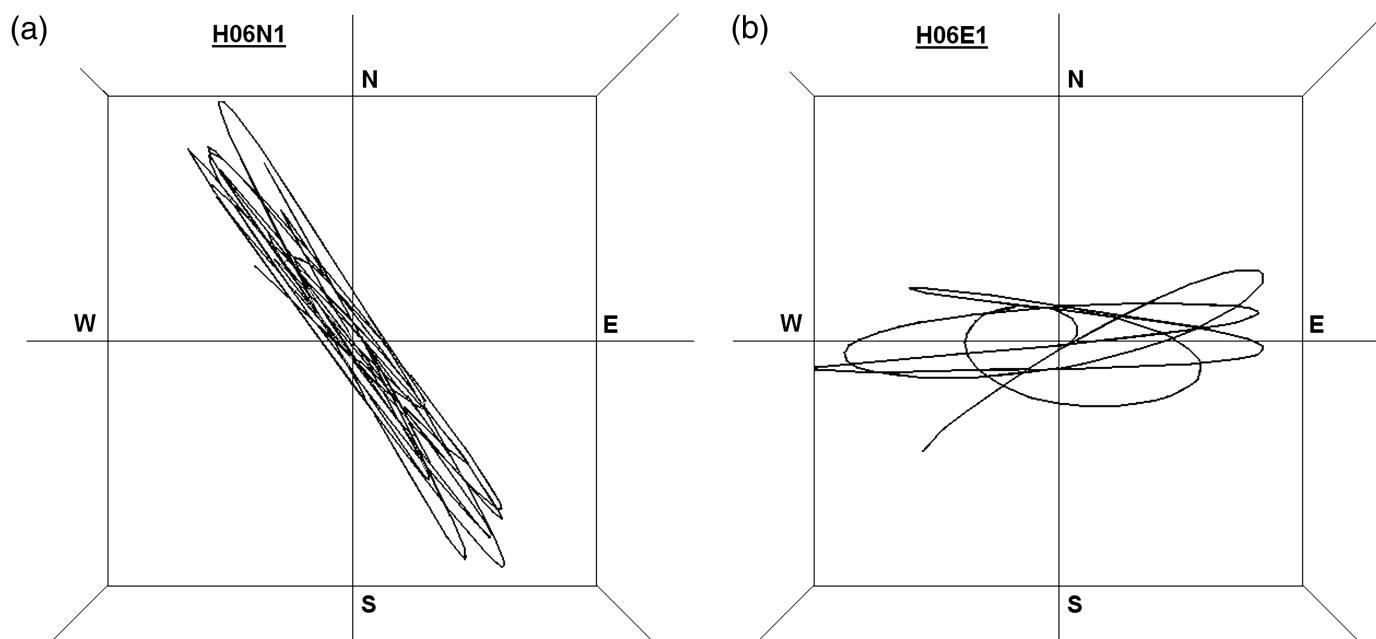
▲ **Figure 9.** Long-period observations record at stations H06N1 and H06E1 in the 0.001–0.004 Hz frequency band from the Samoa islands event. The time of the beginning of fluctuations is marked by the cursor.

the tsunami is 180 m/s (650 km/h), close to the value for the Maule event. The period of the recorded fluctuations is less than for Maule event record, 300 s at the northern station and 280 s at the eastern station. The ratio of the maximum amplitudes of the fluctuations along the direction of polarization at the two station locations is also very similar for the two events, which comforts our interpretation.

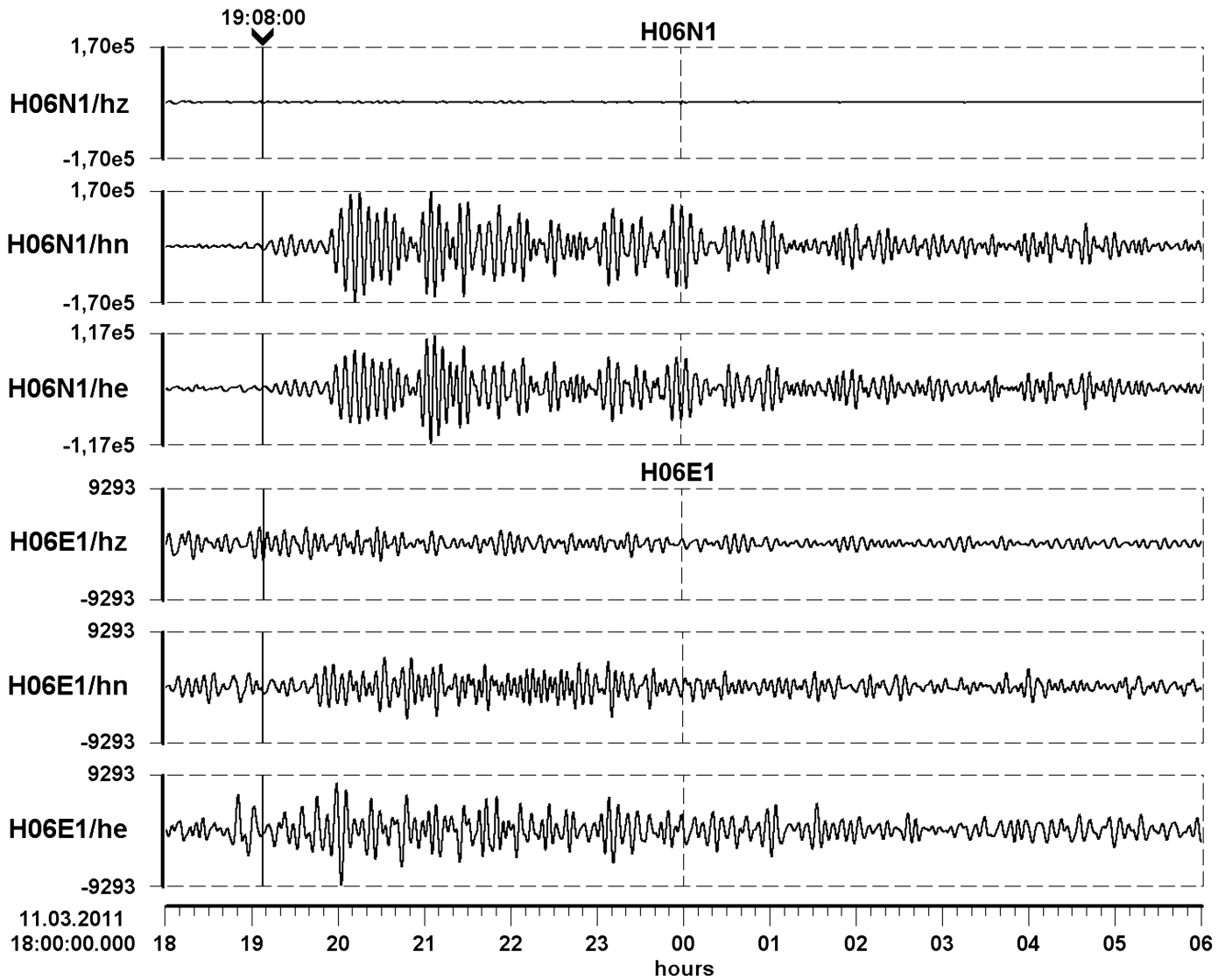
An essential difference between the two tsunamis as seen at station H06 is the direction of arrival of the tsunami wave train. The back azimuth in the Samoa case is 245° as the event is located to the southwest of the island. Both stations H06N1 and H06E1 are on the opposite side of the island. According to our interpretation of the physics of generation of these fluctuations, this should not affect the orientation of movement of fluctuations recorded at the stations at tsunami-arrival time. We will check this using the polarization analysis of the records in the passband 0.001–0.004 Hz. The estimate of the orientation of the fluctuations  $\alpha(t)$  is 140°. This value is very close to the previous result of 148°. The hodograph of movements of the end of the displacement vector is presented in Figure 10a. The orientation of the fluctuations at station H06E is identical to the previous result of 89°. The hodograph in Figure 10b confirms it. Note that the direction of polarization at the northern station in this case is not as stable as in the Maule event case and fluctuates about 10° around a mean value of 148. The linearity of the polarization remains still high, however. This observation argues to the possible presence of smaller amplitude and longer period component (1000–1500 s) with a polarization oriented perpendicularly to the main direction of fluctuation that approximately coincides with the direction to the source. It may be the gravitational wave connected with the main direction of propagation and the period of the tsunami in

the deep open ocean that Okal (2007) observed with bottom seismometers. It would be difficult to differentiate two possible components in the case of the Chilean tsunami because of the coincidence of the two directions in that case.

The catastrophic Japanese event of 11 March 2011 supplements the set of tsunamis observed at H06 and adds one more example of tsunamigenic source with a different azimuth on the Pacific rim (the back azimuth to the source is 311°). The  $M_w$  9.0 magnitude (according to USGS, <http://earthquake.usgs.gov/earthquakes/eqarchives/poster/2011/20110311.php>, last accessed March 2013) of this source is the most powerful of the three events considered and exceeds the magnitude of the Maule event ( $M_w$  8.8). The tsunami generated by the earthquake caused an accident at the Fukushima nuclear plant in Japan and propagated all over the Pacific region and beyond. Station H06 successfully recorded that tsunami. Long-period records at stations H06N1 and H06E1 are presented in Figure 11 in the same frequency band as the previous cases. The propagation time of the tsunami to Socorro Island (observed and theoretical) roughly equals 13 h 30 min. The maximal intensity of the fluctuations at the north station is slightly lower than in the Maule case in spite of the larger magnitude. This may be explained by geometric spreading due to the considerably greater distance from the source (about 90°). On records of H06N1 three clear wave trains are characterized by amplitude increasing with time. They may be the result of interference and reflection of the tsunami wave during its propagation. The intensity of the fluctuations on H06E1 is substantially smaller than at H06N1. They were apparent only after filtering. The Japanese tsunami is unique among the three tsunamis examined because we could observe fluctuations on the south station H06S1 equipped with short-period sensor after low-pass



▲ **Figure 10.** Particle-motion hodograph in the horizontal plane for the long-period fluctuations (0.001–0.004 Hz) at (a) station H06N1 and (b) station H06E1 from the Samoa islands event.



▲ **Figure 11.** Long-period observations record at stations H06N1 and H06E1 in the 0.001–0.004 Hz frequency band from the 11 March 2011, Japanese event. The time of the beginning of the fluctuations is marked by the cursor.

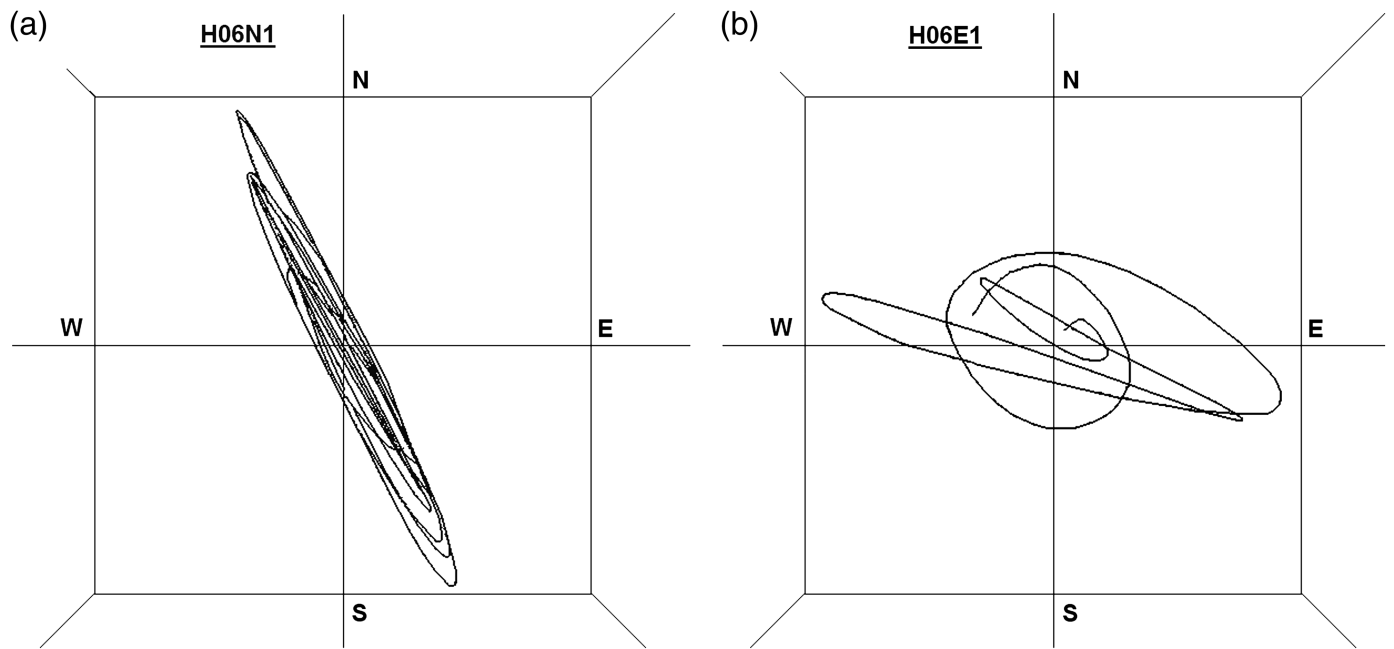
filtering. It might be explained by the orientation of the harbor to the west taking into account the station location near the southern shore of the harbor (see Fig. 1). This direction approximately coincides with the direction of tsunami propagation that could considerably enhance the height of the tsunami in the harbor. The direction of the oscillations in the horizontal plane is also perpendicular to the coastline.

Polarization analysis of three component records at H06N1 leads to the same observations of horizontal fluctuations with a stable azimuth perpendicular to the coastline and equal to  $155^\circ$ , a high rectilinearity and a low inclination angle. These features are characteristic of the passage of a tsunami wave by the island as shown in the previous observations. On average, the polarization of the fluctuations at the H06E1 station is deflected slightly clockwise when compared to the other two events and equal to  $110^\circ$ , which is perpendicular to southeast coast (the corresponding hodographs are presented in

Fig. 12), and which might also be explained by the effect of the gravitational wave as in the Samoa case.

## SUMMARY

As pointed out by Okal (2007), the research presented in his paper as well as this provides an indication that the IMS T-station H06, and similar other IMS and non-IMS stations situated on islands or close to shore may be of value to Tsunami Warning Centers by directly detecting tsunami waves and providing additional data points of the progression of a tsunami. Our interpretation of the physical genesis of these fluctuations supplements works of Okal and other authors. Contrary to their observations, which relied on a larger number of observations at widely separated stations, we had the opportunity to observe the phenomenon at two closely spaced stations (separated by about 11 km) on the same island. Our observation of



▲ **Figure 12.** Particle-motion hodograph in the horizontal plane for the long-period fluctuations (0.001–0.004 Hz) at (a) station H06N1 and (b) station H06E1 from the Japanese event.

the polarizations of the fluctuations at the two H06 seismometers for the three different tsunamis is consistent with local tilt of the coastline area in a direction perpendicular to the coast and inconsistent with a tilt in a direction perpendicular to the propagation of the tsunamis. The unique location of station H06N1 may be effective in recording tsunamis generated by subduction events of the Pacific region. Further work to confirm the assumptions and the physical model explaining the observations at H06 may be of interest and of value to envision the use of this station and similar insular or coastal stations for tsunami warning. To confirm our theory about the generation of long-period motions at H06, it would be of interest in further work to observe additional tsunami wave (from different tsunamigenic events) arrivals at the station and establish that the polarization is independent of the location of the event, but rather is controlled by the geometry of the island's coast. It should also be noted that once this is established, the signal from the tsunami could be separated from noise using this unique polarization. It would be also of value to observe tsunamis at additional long-period seismometers located close to shore. The variation of these observations with increasing distance from shore would also give further precision to the nature and amplitude of the phenomenon. Because we conclude that water loading is the driving mechanism of the observed tilt, it would also be of interest to look at the effect of ocean tides loading on nearshore tiltmeters and horizontal components of long-period seismometers (Farrell, 1972). ☒

## ACKNOWLEDGMENTS

We are grateful to our CTBTO colleagues Jeff Given, Spilio Spiliopoulos, and Mark Prior for discussions and encourage-

ments, Yuri Starovoit for help in quantitative assessment of our observations, as well as Lassina Zerbo for review. In particular, Spilio Spiliopoulos pointed us to the paper by Okal (2007), which made us aware that we were not the first to observe the passage of tsunamis on seismometers and which comforted us on several aspects of our observations. We also thank Emile Okal who reviewed an earlier version of this paper and whose comments and deep insight into the propagation characteristics of tsunami helped us correct a few mistakes and improve this manuscript.

## REFERENCES

- Beavan, J., X. Wang, C. Holden, K. Wilson, W. Power, G. Prasetya, M. Bevis, and R. Kautoke (2010). Near-simultaneous great earthquakes at Tongan megathrust and outer rise in September 2009, *Nature* **466**, 959–963.
- Bridge, J., and R. Demicco (2008). *Earth Surface Processes, Landforms and Sediment Deposits*, Cambridge University Press, Cambridge, UK, 815 pp.
- Farrell, W. E. (1972). Deformation of the Earth by surface loads, *Rev. Geophys. Space Phys.* **10**, 761–797.
- Fritz, H. M., J. C. Borrero, C. E. Synolakis, E. A. Okal, R. Weiss, V. V. Titov, B. E. Jaffe, S. Foteinis, P. J. Lynett, I-C. Chan, and P. L.-F. Liu (2011). Insights on the 2009 South Pacific tsunami in Samoa and Tonga from field surveys and numerical simulations, *Earth Sci. Rev.* **107**, 66–75.
- Gilbert, F. (1980). An introduction to low-frequency seismology, in *Proc. Intl. School Phys., Enrico Fermi*, Course 78, A. M. Dziewonski and E. Boschi (Editors), North Holland, Amsterdam, The Netherlands, 41–81.
- Hanson, J. A., and J. R. Bowman (2005). Dispersive and reflected tsunami signals from the 2004 Indian Ocean tsunami observed on hydrophones and seismic stations, *Geophys. Res. Lett.* **32**, no. 17, L17606, 5 pp.

- Kalkan, E., and V. Graizer (2007). Coupled tilt and translational ground motion response spectra, *J. Struct. Eng.* **133**, no. 5, 609–619.
- Kato, T., Y. Terada, H. Nishimura, T. Nagai, and S. Koshimura (2011). Tsunami records due to the 2010 Chile earthquake observed by GPS buoys established along the Pacific coast of Japan, *Earth Planets Space* **63**, e5–e8.
- Okal, E. A. (2007). Seismic records of the 2004 Sumatra and other tsunamis: A quantitative study, *Pure Appl. Geophys.* **164**, 325–353.
- Pan, C. (1971). Fundamental statistical techniques for the analysis of earth tides, *Bull. Seismol. Soc. Am.* **61**, 203–215.
- Prior, M., A. Poplavskiy, R. Le Bras, and J. Given (2010). Enhancing the contribution of the T-stations of the IMS hydroacoustic network to IDC processing and tsunami warning, in *Proc. 2010 Monitoring Research Review: Ground-Based Nuclear Explosion Monitoring Technologies*, LA-UR-10-05578, Vol. II, 558–564.
- Rodgers, P. (1968). The response of the horizontal pendulum seismometer to Rayleigh and Love waves, tilt, and free oscillations of the earth, *Bull. Seismol. Soc. Am.* **58**, 1385–1406.
- Shevchenko, V. P. (2002). Methodological principles of differential polarization analysis of vector signals, *Meas. Tech.* **12**, 14–17.
- Valenzuela, R. W., Javier F. Pacheco, José Pereira, Jorge A. Estrada, Jesús A. Pérez, José L. Cruz, Dario Baturan, Arturo Cárdenas, and José A. Santiago (2007). The seismic and hydroacoustic stations on Socorro Island: Early results, *Geofisc. Int.* **46**, no. 1, 3–18.
- Yuan, X., R. Kind, and H. Pedersen (2005). Seismic monitoring of the Indian Ocean tsunami, *Geophys. Res. Lett.* **32**, no. 15, L15308, 4 pp.

*Alexander S. Poplavskiy*

*Ronan J. Le Bras<sup>1</sup>*

*Comprehensive Nuclear-Test-Ban Treaty Organization*

*Vienna International Centre*

*P.O. Box 1200*

*1400 Vienna, Austria*

---

<sup>1</sup> Now at Institut für Meteorologie und Geophysik, Universität Wien, UZA II, Ebene 5, Althanstrasse 14, 1090 Wien, Austria.